Determination of Launch-Vehicle Response to Detailed Wind Profiles

HAROLD C. LESTER* AND HOMER G. MORGAN†
NASA Langley Research Center, Hampton, Va.

A method for predicting the response and bending loads experienced by a launch vehicle ascending through winds is presented. The horizontal wind-velocity profiles utilized by the method are those which are measured by a high-resolution technique, such as the smoke-trail method, and contain high-frequency gust components as well as the longer wavelength winds and wind shears. Motion in the pitch plane is considered, and structural bending and propellant slosh degrees of freedom are included in the analysis. A body-fixed coordinate system is used, and a variational principle is employed to derive the nonlinear differential equations of motion, which have time-varying coefficients. The equations are solved numerically by means of a Runge-Kutta procedure. The wind-disturbed flat-earth ascent trajectory is computed for a specified pitch program. The method is applied to a representative launch vehicle, and its response and dynamic loads are determined for flight through a typical wind profile.

Nomenclature

$C_{N\alpha}(M)$ = slope of the normal-force coefficient, 1/rad
H, R = inertial axes
h, r = coordinates along inertial axes denoting altitude and range, respectively, ft
L = length of launch vehicle, ft
M = Mach number, dimensionless
m_k = propellant slosh mass, lb-sec²/ft
q = dynamic pressure, $q = \frac{1}{2}\rho V_{mw}^2$, psf
$q_i(t)$ = generalized coordinate associated with the ith bending mode ($i = 1, 2,$ and 3), ft
$u(x, t)$ = elastic displacement of structural center line, equal to $\sum_i \phi_i(x)q_i(t)$, ft
V_m = c.g. velocity of launch vehicle, fps
V_{mw} = velocity of launch vehicle relative to wind, fps
V_w = wind velocity, fps
V_x, V_y = components of c.g. velocity vector along X and Y axes, respectively, fps
X, Y = body-fixed coordinate axes
x, y = coordinates along X and Y body axes, ft
x_{cg} = gravity center coordinate, ft
x_k = propellant slosh mass location, ft
$x_\theta, x_{\dot\theta}$ = coordinates locating attitude sensor and attitude-rate sensor, respectively, ft
α = rigid-body angle of attack, equal to $\theta - \gamma$, rad
α_w = wind-induced angle of attack, rad
γ = flight-path angle, rad
δ = gimbaled engine deflection angle, rad
δ_c = gimbaled engine command function, rad
θ, θ_c = attitude and attitude command angle, respectively, rad
θ_f = feedback angle, rad
θ_e = error angle, equal to $\theta_c - \theta_f$, rad
λ_k = propellant slosh coordinate as measured from deformed structural centerline, ft
ρ = atmospheric density at altitude h, lb-sec²/ft⁴
$\phi_i(x)$ = displacement of ith mode, dimensionless
$\dot{(\ )}$ = a differentiation with respect to time
$(\ )'$ = a differentiation with respect to x

Presented as Preprint 64-82 at the AIAA Aerospace Sciences Meeting, New York, January 20–22, 1964; revision received July 13, 1964.

* Aerospace Technologist, Dynamic Response Section, Dynamic Loads Division.

† Aerospace Technologist Dynamic Response Section, Dynamic Loads Division. Associate Fellow Member AIAA.

Introduction

As a launch vehicle ascends through the atmosphere, it is subjected to many disturbances among which are wind velocities, which have been referred to as winds, wind shears, and gusts. The loads induced on the structure by these atmospheric disturbances are a major part of the total flight loads for which the vehicle must be designed. Therefore, the dynamic responses and loads due to the wind velocities must be predictable and understood to assure optimum design of an adequate structure.

Methods that have been used to determine wind, wind shear, and gust loads have been influenced by the types of data on atmospheric disturbances that were available. These data are of two types: radiosonde balloon measurements of horizontal wind-velocity profiles and vertical gust-velocity measurements made by horizontally flying airplanes. The former data describe the long wavelength behavior of the atmosphere (winds and wind shears), whereas the latter data represent short wavelength fluctuations.

Many methods used for predicting loads make use of rigid-body representations for the vehicle flying through balloon-measured wind profiles.[1–5] Loads obtained from relatively arbitrary one-minus-cosine gusts or random gusts acting on a flexible vehicle are then superimposed on the wind loads to obtain total loads. Recently, several methods have been developed for determining wind and wind shear loads on a flexible vehicle. For example, Goldman[6] and Keith, Lincoln, and Tarnower[7] have presented solutions for perturbations from a reference trajectory. Clingan, Gates, and Andrews[8] use a direct numerical solution of differential equations having time-dependent coefficients. However, these methods still rely on superposition of a gust load from a separate analysis to obtain total loads.

In this paper, a method for determining the response and bending-moment loads on a launch vehicle ascending through detailed wind profiles is presented. The wind profiles utilized contain both the long wavelength winds and wind shears and the short wavelength gusts. This method is required because detailed wind-profile data, obtained by the smoke-trail technique,[9] are now becoming available. To properly use these data, the method represents the launch vehicle by a set of nonlinear differential equations having time-varying coefficients and includes elastic bending, propellant sloshing, and control-system effects. The response equations are solved

numerically on a digital computer. Inherent in the solution is the wind-disturbed ascent trajectory. The method is illustrated by application to a typical launch vehicle.

Wind-Profile Data

The methods used to calculate the wind loads on launch vehicles are influenced by the type of wind-profile data.[10] The three types of wind profiles which have been used for loads calculations are illustrated in Fig. 1, where wind velocity is shown as a function of altitude. The principal source of data has been radiosonde balloon soundings, typically illustrated by the broken line. In this method, a lightweight balloon is tracked by radio direction finding equipment as it ascends through the atmosphere. The tracking data are averaged over 1000- or 2000-ft-alt intervals, thus masking the short wavelength fluctuations. Many wind soundings of this type have been made over the past decade at a large number of geographical locations. Some of the more recent load prediction methods[2–5] use these wind profiles directly to determine the statistics of expected wind loadings by analytically flying a vehicle through a large number of profiles. Other work[11–13] has attempted to account for the statistical character of the atmosphere by using the sounding data to generate synthetic wind profiles, such as that illustrated by the dashed line in the figure. Since the synthetic profiles are deduced from the radiosonde data, the short wavelength fluctuations, or gusts, are not included in such profiles.

More recently, techniques such as the smoke-trail method have been developed which measure detailed wind profiles illustrated by the solid curve. These wind-sounding methods provide wind-velocity readings at 50- to 100-ft-alt intervals, compared to the 1000- to 2000-ft-alt averaging increments used in balloon techniques, and thus define the short wavelength disturbances, or gusts, as well as the winds and wind shears. Only a limited number of the detailed profiles are available at present. However, sounding rocket programs to obtain enough profiles for statistical evaluation are in progress. The method of loads calculation presented herein has been developed to utilize these detailed wind-profile data.

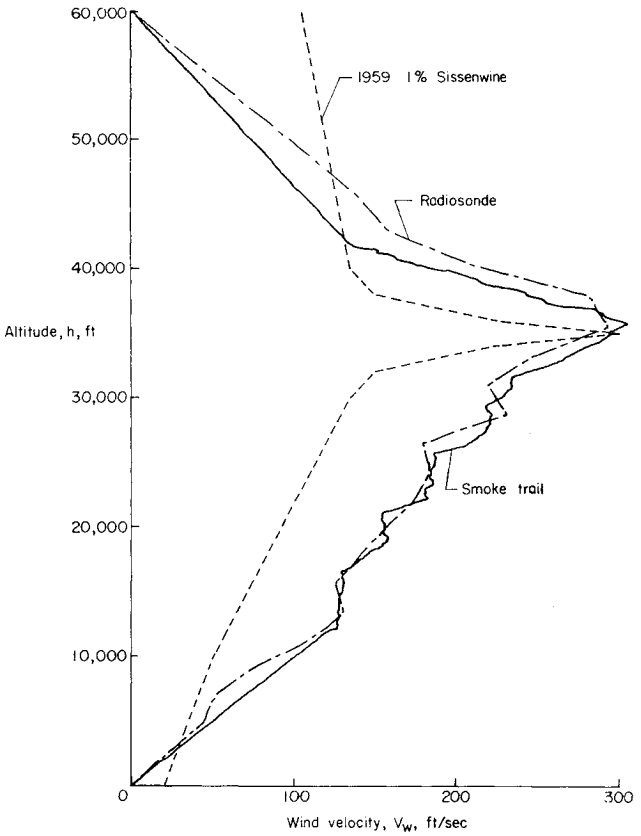

Fig. 1 Types of wind profiles.

Analysis

The procedure will be outlined very briefly since the details can be found in the literature.

Mathematical Model

The coordinate systems are illustrated in Fig. 2. Both body-fixed and inertial (space-fixed) axes are used. In general, motion is referenced to a Cartesian coordinate system (X, Y) fixed in the undeformed rigid body and oriented with respect to the local flat earth horizontal (R inertial axis) by the attitude angle θ. The velocity vector of the center of gravity is oriented to the local horizontal by γ, the flight-path angle. The rigid-body motion is characterized by translatory motion along the respective body axes and a rotation about the c.g. The time rate of change of the c.g. within the vehicle is neglected.

The vehicle is assumed to be autopilot controlled and subjected to the disturbing influence of atmospheric winds. Control forces are produced by vectoring the thrust chambers through an angle δ in response to commands provided by the autopilot.

Bending of the launch-vehicle's structure is approximated by the superposition of several free-free beam modes, using the relation

$$u(x, t) = \sum_i \phi_i(x) q_i(t)$$

which defines the centerline displacement (see Fig. 2) of the vehicle's structure, where $\phi_i(x)$ represents the free-free beam modes and $q_i(t)$ represents the related generalized coordinates. The mode shapes $\phi_i(x)$ are functions of the mass and stiffness properties exhibited at discrete times in the trajectory.

A spring-mass analogy is employed to approximate liquid propellant motion. This analogy has been developed in the literature[1, 14] for a variety of tank configurations. It duplicates the force exerted on the tank by the liquid when the fundamental slosh mode is excited at its resonant frequency. The parameters required by this representation are slosh mass (m_k), slosh frequency (ω_k), and slosh mass location (X_k). The quantities are, in general, functions of the acceleration field and fluid depth-tank radius ratio, which may be correlated to time using the propellant flow rates, and may be evaluated from information available in the cited literature. Viscous damping is included in each slosh degree of freedom.

The gimbaled thrust chamber or engine is positioned by an actuator in response to commands from the control system. Generally, the actuator is an electrohydraulic mechanism that exhibits a nonlinear response at small amplitudes. For the

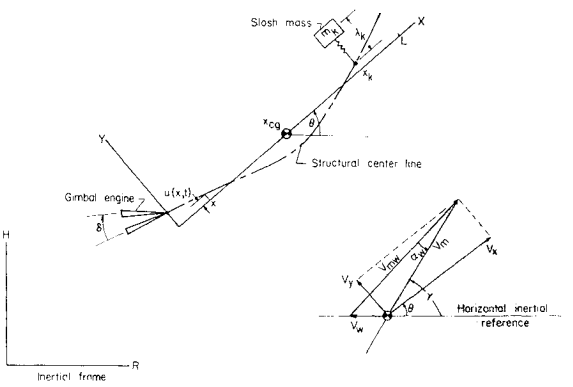

Fig. 2 Coordinate system and velocity vector relations.

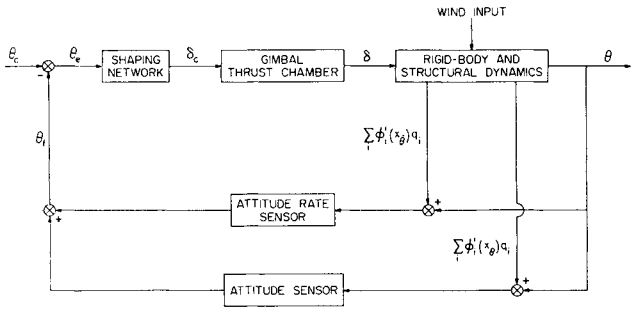

Fig. 3 Control-system block diagram.

present analysis, the positioning mechanism is assumed to be described by a third-order, linear differential equation with the coefficients determined by a linearization technique such as the describing function method.[15]

Method of Analysis

The equations of motion are derived using a variational principle founded on momentum considerations.[16] The equations that result from this principle are

$$\frac{d}{dt}\left(\frac{\partial L}{\partial \dot{\beta}_i}\right) - \frac{\partial L}{\partial \beta_i} = Q_{\beta_i} + \bar{Q}_{\beta_i} \tag{1}$$

Here, L is the Lagrangian, defined as the difference between the kinetic energy T and potential energy U, and β_i is any generalized coordinate. The generalized forces Q_{β_i} and $\bar{Q}_{\beta_i}$ result from external forces not derivable from a potential and internal forces due to mass flow within the system, respectively. Note that, if mass-flow effects are neglected ($\bar{Q}_{\beta_i} = 0$), Eq. (1) reduces to the classical form of Lagrange's equation.

The general form of the Lagrangian operator is referred to an inertial or space-fixed frame. It is convenient, however, to describe the motion in terms of a reference frame that is fixed to and moves with the launch vehicle, such as the (X, Y) coordinate system illustrated in Fig. 2. It is therefore necessary to transform the classical expression of Lagrange's equations to an equivalent form valid in the rotating coordinate system. Details of this transformation to "quasi-coordinates" may be found in the literature.[17, 18] A similar but less general form is developed by Thomson[19] from virtual work considerations. When transformed, Lagrange's equations for the rigid-body

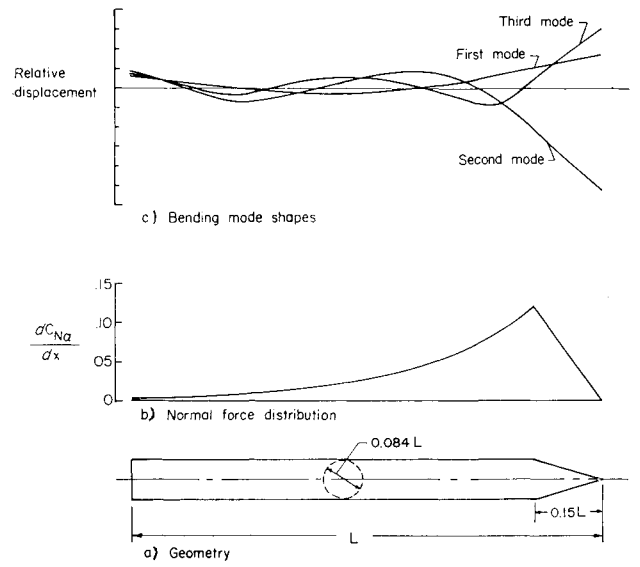

Fig. 4 Launch-vehicle configuration at 62 sec after liftoff.

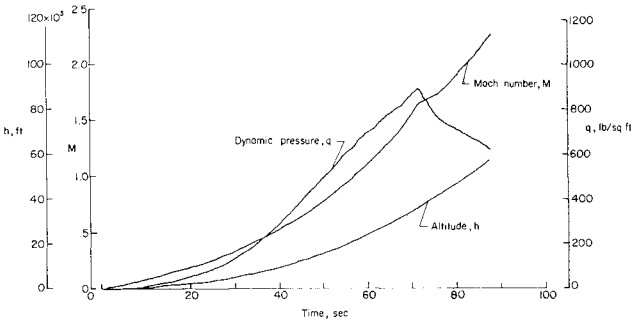

Fig. 5 Altitude, Mach number, and dynamic pressure time histories.

degrees of freedom (translation and pitch) assume the following forms:

$$\left.\begin{aligned}
&\frac{d}{dt}\left(\frac{\partial T}{\partial \dot{V}_x}\right) - \dot{\theta}\left(\frac{\partial T}{\partial V_y}\right) + \sin\theta\left(\frac{\partial U}{\partial h}\right) = \Sigma F_x \\
&\frac{d}{dt}\left(\frac{\partial T}{\partial \dot{V}_y}\right) + \dot{\theta}\left(\frac{\partial T}{\partial V_x}\right) + \cos\theta\left(\frac{\partial U}{\partial h}\right) = \Sigma F_y \\
&\frac{d}{dt}\left(\frac{\partial T}{\partial \dot{\theta}}\right) + V_x\left(\frac{\partial T}{\partial V_y}\right) - V_y\left(\frac{\partial T}{\partial V_x}\right) + \frac{\partial U}{\partial \theta} = \Sigma M_{cg}
\end{aligned}\right\} \tag{2}$$

where U has been assumed independent of r. The generalized forces (ΣF_x, ΣF_y, and ΣM_{cg}) account for all external forces and moments not included in the potential function U. Lagrange's equations for the remaining degrees of freedom are invariant under the transformation and have the form

$$\frac{d}{dt}\left(\frac{\partial T}{\partial \dot{\beta}_i}\right) - \left(\frac{\partial T}{\partial \beta_i}\right) + \left(\frac{\partial U}{\partial \beta_i}\right) + \left(\frac{\partial D}{\partial \dot{\beta}_i}\right) = \Sigma Q_{\beta_i} \tag{3}$$

where β_i represents a particular coordinate (degree of freedom) and D, a velocity-dependent dissipation function, has been included as a convenient way to account for internal damping.

The details of forming the kinetic and potential energies and the dissipation function and carrying out the operations indicated by Eqs. (2) and (3) will not be repeated here since they can be found in the references.[16, 20]

Aerodynamic and Propulsive Forces

Aerodynamic forces are quasi-steady, based on the local time-dependent angle of attack and normal-force distributions measured or calculated along the launch-vehicle longitudinal axis. These forces are assumed linear with angle of attack and neglect the gust penetration effect. The aerodynamic forces are functions of Mach number but are converted to functions of time for use in the analysis by a Mach number-time relation from a nominal trajectory.

As noted earlier, the variational principle yields generalized forces that account for distributed loadings due to the momentum flux of the internal propellant flow. The distributed loading, when integrated, yields the primary propulsion or thrust forces and additional damping terms that may be categorized as jet damping effects. Jet damping is neglected herein and only the principal thrust terms are retained in the equations of motion.[20]

Control-System Considerations

A general description of launch-vehicle control systems has not been attempted due to the large variety of possible combinations of elements. Instead, a typical autopilot control system was chosen to illustrate the approach with the realization that the control-system equations would probably have to be rewritten for a particular launch vehicle. The block

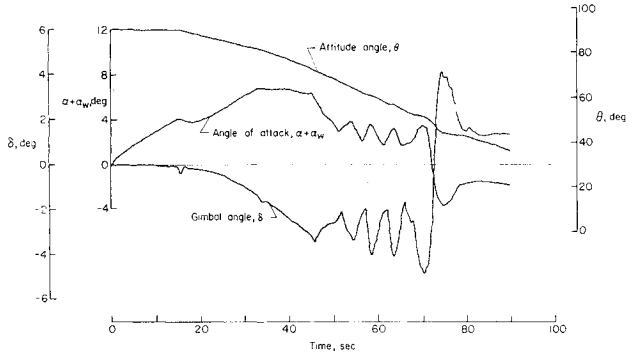

Fig. 6 Attitude angle, angle-of-attack, and gimbal angle time histories.

diagram of the autopilot used is shown in Fig. 3. Pitch attitude commands are the system inputs. The forward loop contains a signal shaping network consisting of a second-order filter in parallel with an integrator. The gimbaled engine is a third-order, linear system. Control-system feedback is through two paths: an attitude channel and an attitude-rate channel. The terms proportional to g_i represent the structural motion that is sensed by the gyros (structural feedback).

Computer Program

The launch-vehicle wind-response equations were programed for solution on a high-speed digital computer. The program has provisions for as many as three bending and two propellant slosh degrees of freedom. Time-dependent input parameters were approximated using tabulated data and a linear interpolation subroutine. In order to accommodate detailed wind inputs, the wind (V_w) table was expanded to facilitate defining the wind velocity at as many as 1000 discrete altitude levels. For example, with an altitude ceiling of 60,000 ft, the wind input V_w may be defined about every 60 ft of altitude, although the table may be compressed in certain altitude intervals and expanded in others to provide maximum definition. Atmospheric properties were interpolated from a standard atmosphere.

The nonlinear, time-dependent equations were solved by a fifth-order integration using a fourth-order Runge-Kutta routine. The dependent variables (velocities and displacement) were computed for both a whole and two half-intervals and the results compared to establish whether the computing interval should be halved, doubled, or remain unchanged. Furthermore, on the basis of the difference between the whole- and two half-increment computations, the latter was improved by a correction procedure known as extrapolation to zero interval size.[21] Double precision internal addition was used to reduce round-off error. Since the equations are linearly cross-coupled through the accelerations, a matrix inversion was required to obtain these quantities.

Application to a Typical Launch Vehicle

In order to illustrate this method of determining wind loads, the response of a typical launch vehicle was calculated. This portion of the paper will be devoted to this calculation study as illustrative of the results that can be obtained by the procedure.

Configuration

The configuration chosen for the study is shown in Fig. 4. Its characteristics were those of a large liquid-propellant launch vehicle having a thrust equal to 1.25 times its weight at liftoff. The trajectory has a 15-sec vertical rise followed by an attitude-time schedule that approximated a no-wind zero-lift trajectory. The vehicle was represented by three elastic, two sloshing, and three rigid-body degrees of freedom. The control system had attitude and attitude-rate feedback, and an integration of the attitude error and a second-order filter in the forward loop.

Aerodynamically, the configuration is a cone cylinder. Lift, drag, and moment data for this configuration were available for the Mach numbers of interest. However, lift distributions, such as the one illustrated for a Mach number of about 1.0, were determined by assuming a linear lift build-up over the forebody and an exponential decay over the afterbody.

The elastic properties of the vehicle are illustrated by the mode shapes at 62 sec after liftoff as shown in Fig. 4. Both the mode shapes and the frequencies of the modes changed with time, i.e., the first-mode frequency increased from 2.01 cps at liftoff to 2.58 cps at 100 sec of flight.

Response to Detailed Wind Profiles

The launch vehicle was flown analytically through the smoke-trail wind profile shown in Fig. 1. The responses discussed in this section are typical examples of the results obtainable from this procedure using measured wind data.

Trajectory

The wind-disturbed trajectory of the vehicle is computed as part of the solution to the equations of motion. The trajectory is illustrated in Fig. 5 for flight through the smoke-trail wind (headwind). Maximum dynamic pressure is about 900 psf about 72 sec after liftoff. The corresponding Mach number is about 1.65 and the altitude is about 36,000 ft. The horizontal wind velocity combines vectorially with the inertial vehicle velocity to influence these quantities as evidenced by the slight peaking of dynamic pressure and Mach number. The calculations have been carried to 90 sec of flight time (about an altitude of 60,000 ft), well beyond maximum dynamic pressure and the peak loading conditions.

Other significant trajectory time histories for flight through the same wind profile are shown in Fig. 6. The attitude angle indicates a vertical rise for 15 sec, then a gradual tilt as commanded by the pitch program. Small attitude oscillations are apparent in the region of max q. These oscillations also appear in the total angle-of-attack time history. They occur at the pitch frequency of the vehicle and are excited by several sudden, almost step, changes in wind velocity that appear in Fig. 1. Angles of attack of about 7° occur early in the flight during the initiation of the pitch program. Near max q, the peak angles of attack are about ±4°. The gimbal angle δ follows the angle of attack very closely and has maximum values of about $\pm 4\frac{1}{2}°$. A slight high-frequency response appears in the gimbal angle time history, indicating structural coupling.

Elastic-body response

The response of the elastic degrees of freedom is shown in Fig. 7. The curves are time histories of the displacement of

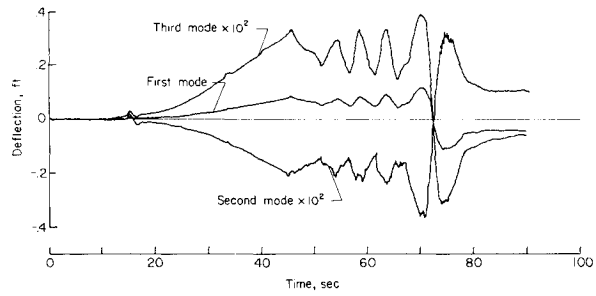

Fig. 7 Time histories of the deflections of the first three bending modes at the gimbal station.

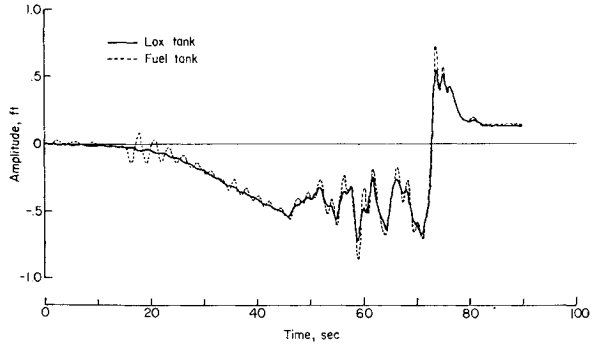

Fig. 8 Sloshing response of propellants.

the gimbal station in each of the three bending modes. On this time scale, the oscillations at the modal frequencies are barely visible so that most of the response appears to be quasi-static and follows the gimbal angle and angle-of-attack time histories. The maximum displacements occur near max q and amount to less than 0.15 ft in the first mode at the gimbal station. Displacements of the second and third modes are two orders of magnitude less than first-mode displacements.

Sloshing responses

The responses of the two slosh masses are illustrated in Fig. 8. The solid curve is the time history of slosh motion in the LOX tank, whereas the dashed line is the time history for the fuel motion. The low damping of the slosh freedoms (about 5% of critical) is apparent from the persistence of the oscillations. The fuel is excited to much higher slosh amplitudes than the sloshing LOX: a fact explained by noting that the fuel tank is farthest from the vehicle center of gravity and subjected to larger excitation as the vehicle pitches. No sloshing instability is evident, a result that would be expected for an adequate control system.

Bending-moment responses

Examples of the bending-moment response of the vehicle as it flies through the smoke-trail profile are shown in Fig. 9. The upper curve, labeled station 1, is the bending moment at a point about 15% of the vehicle length forward of the aft end. The lower curve for station 2, located about one-third of the length from the aft end, is in the region of maximum bending moment on the vehicle, and all bending moments are normalized to its peak value. The apparent oscillations in the time period from 40 to 70 sec correspond to the oscillations in attitude and angle of attack, which were induced by the wind. The large reversal in bending moment which occurs at about 75 sec results from the large wind shear reversal between 35,000 and 40,000 ft (Fig. 1). The peak bending moments seem to occur near this shear reversal.

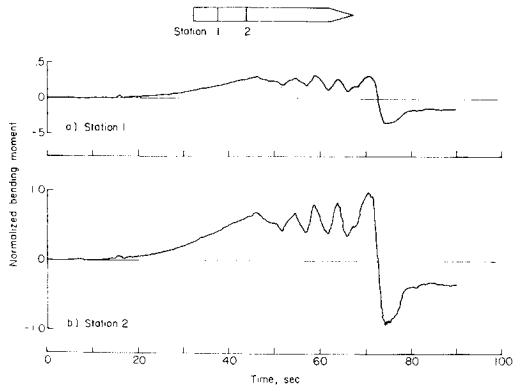

Fig. 9 Bending-moment time histories at two vehicle locations.

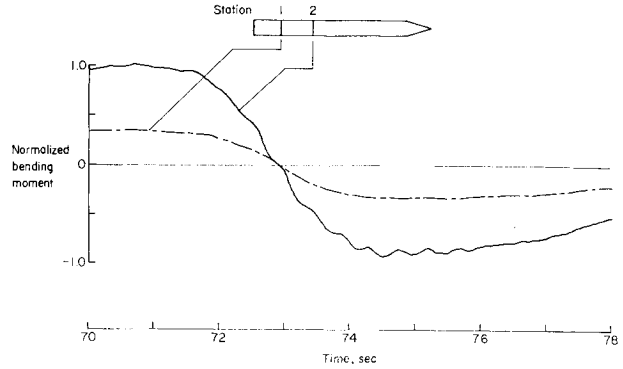

Fig. 10 Bending-moment time histories near the wind shear reversal.

The bending-moment responses on this time scale, showing 90 sec of flight time, reveal very little excitation of the bending modes. Only a few oscillations appear to be excited by the wind shear reversal at about 75 sec. In Fig. 10, that portion of the bending-moment response near the wind shear reversal, from 70 to 78 sec, has been replotted on an expanded scale. Here, the excitation of the bending modes is more apparent, especially at the forward station. The aft station is nearer the first-mode nodal point and is not noticeably affected. The modal response produces only a small percentage increase in the total bending load experienced even for the forward station. This can be attributed to the particular wind profile chosen for this sample calculation: a profile having a very high peak wind of over 300 fps, but having a very low turbulence content. Another profile, containing higher turbulence or gust levels, would be expected to produce larger modal excitation.

Concluding Remarks

A method for calculating the dynamic response and loads of a launch vehicle ascending through detailed wind-velocity profiles has been presented. Even though the procedure is quite detailed, several effects of possible significance have been omitted. For example, future experience with flight loads may show that three-dimensional analyses are required, especially for vehicles carrying winged or asymmetric payloads with aerodynamic or modal coupling between the pitch and yaw planes. Another example is the penetration of the vehicle into a gust front, neglected herein but possibly important for response to short wavelength disturbances.

This method of loads prediction will be quite valuable as a final design tool to check the loads generated on a vehicle by "worst case" detailed wind-velocity profiles. The method will also be required when good quality flight loads data on launch vehicles become available and calculations to check experiment against analysis are attempted.

References

[1] Lukens, D. R., Schmitt, A. F., and Broucek, G. T., "Approximate transfer functions for flexible-booster-and-autopilot analysis," Wright Air Development Div. TR-61-93 (April 1961).

[2] Hobbs, N. P., Criscione, E. S., Mazzola, L. L., and Frassinelli, G. J., "Development of interim wind, wind shear, and gust design criteria for vertically rising vehicles," Wright Air Development Div. TR 59-504 (July 1959); classified.

[3] Mazzola, L. L., Hobbs, N. P., and Criscione, E. S., "Wind, wind shear, and gust design criteria for vertically-rising vehicles as recommended on the basis of Montgomery, Alabama, wind data," Wright Air Development Div. TR 61-99 (1961); classified.

[4] Mazzola, L. L., "Design criteria for wind-induced flight loads on large boosted vehicles," AIAA J. 1, 913–914 (1963).

[5] Mazzola, L. L., Putukian, J., Criscione, E. S., and Hobbs, N. P., "Wind, wind shear, and gust design criteria for vertically-rising vehicles as recommended on the basis of wind data from eleven United States and foreign locations," Aeronautical Systems Div. TDR-62-908 (June 1963); classified.

[6] Goldman, R., "A method for predicting dynamic response of missiles to atmospheric disturbances," IAS Paper 62-40 (January 1962).

[7] Keith, J. S., Lincoln, J. W., and Tarnower, G., "Aeroelastic analyses of multistage rocket systems," AGARD Rept. 390 (July 1961).

[8] Clingen, B. E., Gates, R. M., and Andrews, J. S., "Dynamic loads during booster flight," Aeronautical Systems Div. TDR-63-302 (May 1963).

[9] Henry, R. M., Brandon, G. W., Tolefson, H. B., and Lanford, W. E., "The smoke-trail method for obtaining detailed measurements of the vertical wind profile for application to missile-dynamic-response problems," NASA TN D-976 (1961).

[10] Morgan, H. G. and Collins, D. F., "Some applications of detailed wind profile data to launch vehicle response problems," AIAA J. **1**, 368–373 (1963).

[11] Sissenwine, N., "Windspeed profile, windshear, and gusts for design of guidance systems for vertical rising air vehicles," Air Force Surveys in Geophysics No. 57, Air Force Cambridge Research Center, AFCRC-TN-54-22 (November 1954).

[12] Scoggins, J. R. and Vaughn, W. W., "Cape Canaveral wind and wind shear data (1 through 80 km) for use in vehicle design and performance studies," NASA TN D-1274 (1962).

[13] Henry R. M., "A statistical model for synthetic wind profiles for aerospace vehicle design and launching criteria," NASA TN D-1813 (1963).

[14] Bauer, H. F., "Theory of the fluid oscillations in a circular cylindrical ring tank partially filled with liquids," NASA TN D-557 (1960).

[15] Backus, F. I., "Describing functions for nonlinear electrohydraulic gimbaled rocket-engine position servos with application to closed-loop control systems," Convair Astronautics, Rept. AE60-0287 (June 10, 1960).

[16] Edelen, D. G. B., "On the dynamical effects of fuel flow on the motion of boost vehicles," Rand Corp. Memo. RM-3268-NASA (October 1962).

[17] Whittaker, E. T., *A Treatise on the Analytical dynamics of particles and Rigid Bodies* (Cambridge University Press, Cambridge, England, 1961).

[18] Corben, H. C. and Stehle, P., *Classical Mechanics* (John Wiley and Sons, Inc., New York, 1961).

[19] Thomson, W. T., *Introduction to Space Dynamics* (John Wiley and Sons, Inc., New York, 1961).

[20] Lester, H. C. and Collins, D. F., "Determination of loads on a flexible launch vehicle during ascent through winds," NASA TN (submitted for publication).

[21] Hartree, D. R., "Deferred approach to the limit," *Numerical Analysis* (Oxford University Press, Oxford, England, 1958).

JAN.-FEB. 1965 J. SPACECRAFT VOL. 2, NO. 1

Shocks Induced by Secondary Fluid Injection

HENRY TAO-SZE HSIA,* HOWARD S. SEIFERT,† AND KRISHNAMURTY KARAMCHETI‡
United Technology Center, Sunnyvale, Calif. and
Stanford University, Stanford, Calif.

Studies were conducted to determine the shape of the shock wave when a secondary fluid is injected into a supersonic nozzle. Experiments were done in a supersonic two-dimensional blow-down wind tunnel using nitrogen for the primary flow. Gaseous nitrogen, liquid nitrogen, and Freon-12 were used as the injectants. The shape of the induced shock for different injection conditions was determined by means of schlieren photographs and china-clay streak patterns of the flow on the nozzle wall. The possibility of relating the experimentally observed shock shapes with analytical results obtained by the application of blast-wave ideas was explored. It was shown that, for the experimental conditions investigated, the shock shapes may be predicted satisfactorily by the use of the second-order solution for the blast wave.

Nomenclature

A = area
c = speed of sound
D = diameter
E = energy per unit length
J = const [see Eq. (1)]
$\dot{m}$ = mass flow rate
M = Mach number
p = static pressure
P = stagnation pressure, liquid injection pressure
R = radius of shock
R^* = a characteristic length [see Eq. (3)]
R_c = $\eta^{1/2}R^*$
t = time
V = velocity of flow
x = distance measured from apex of shock along a direction parallel to the nozzle axis
γ = ratio of specific heats
η_1 = correction factor for non-normal injection [see Eq. (4)]
η_2 = correction factor for evaporation and reaction [see Eq. (5)]
η = $\eta_1\eta_2$
θ = angle between injector and nozzle axis
λ = const [see Eq. (1)]
ρ = density

Presented as Preprint 64-111 at the AIAA Solid Propellant Conference, Palo Alto, Calif., January 29–31, 1964; revision received August 24, 1964. This report is based on a thesis submitted by the first author to the Department of Aeronautics and Astronautics, Stanford University, in partial fulfillment of the requirements for the degree of Engineer. The authors wish to acknowledge the collaboration from members in the Physical Sciences Laboratory, United Technology Center, and in particular A. Lavoria, for his assistance in the operation of experiments.

* Staff Scientist; also Graduate Student, Department of Aeronautics and Astronautics. Member AIAA.
† Manager, Physical Sciences Laboratory; also Professor, Department of Aeronautics and Astronautics. Fellow Member AIAA.
‡ Consultant; also Associate Professor, Department of Aeronautics and Astronautics. Associate Fellow Member AIAA.